Are some packings more equal than others? A direct test of the Edwards conjecture

Stefano Martiniani,[1,*] K. Julian Schrenk,[1] Kabir Ramola,[2] Bulbul Chakraborty,[2] and Daan Frenkel[1]

[1] *Department of Chemistry, University of Cambridge, Lensfield Road, Cambridge, CB2 1EW, UK*
[2] *Martin Fisher School of Physics, Brandeis University, Waltham, MA 02454, USA*

arXiv:1610.06328v1 [cond-mat.soft] 20 Oct 2016

In the late 1980s, Sir Sam Edwards proposed a possible statistical-mechanical framework to describe the properties of disordered granular materials. A key assumption underlying the theory was that all jammed packings are equally likely. In the intervening years it has never been possible to test this bold hypothesis directly. Here we present simulations that provide direct evidence that at the unjamming point, all packings of soft repulsive particles are equally likely, even though generically, jammed packings are not. Our results therefore support Edwards' original conjecture. We also present evidence that at unjamming the configurational entropy of the system is maximal.

In science, most breakthroughs cannot be derived from known physical laws: they are based on inspired conjectures [1]. Comparison with experiment of the predictions based on such a hypothesis allows us to eliminate conjectures that are clearly wrong. However, there is a distinction between testing the consequences of a conjecture and testing the conjecture itself. A case in point is Edwards' theory of granular media. In the late 1980s, Edwards and Oakeshott [2] proposed that many of the physical properties of granular materials ('powders') could be predicted using a theoretical framework that was based on the assumption that all distinct packings of such a material are equally likely to be observed. The logarithm of the number of such packings was postulated to play the same role as entropy does in Gibbs' statistical-mechanical description of the thermodynamic properties of equilibrium systems. However, statistical-mechanical entropy and granular entropy are very different objects. Until now, the validity of Edwards' hypothesis could not be tested directly - mainly because the number of packings involved is so large that direct enumeration is utterly infeasible - and, as a consequence, the debate about the Edwards hypothesis has focused on its consequences, rather than on its assumptions. Here we present results that show that now, at last, it is possible to test Edwards' hypothesis directly by numerical simulation. Somewhat to our own surprise, we find that the hypothesis appears to be correct precisely at the point where a powder is just at the (un)jamming threshold. However, at higher densities, the hypothesis fails. At the unjamming transition, the configurational entropy of jammed states appears to be at a maximum.

The concept of 'ensembles' plays a key role in equilibrium statistical mechanics, as developed by J. Willard Gibbs, well over a century ago [3]. The crucial assumption that Gibbs made in order to arrive at a tractable theoretical framework to describe the equilibrium properties of gases, liquid and solids was that, at a fixed total energy, every state of the system is equally likely to be observed. The distinction between, say, a liquid at thermal equilibrium and a granular material is that in a liquid, atoms undergo thermal motion whereas in a granular medium (in the absence of outside perturbations) the system is trapped in one of many (very many) local potential energy minima. Gibbsian statistical mechanics cannot be used to describe such a system. The great insight of Edwards was to propose that the collection of all stable packings of a fixed number of particles in a fixed volume might also play the role of an 'ensemble' and that a statistical-mechanics like formalism would result if one assumed that all such packings were equally likely to be observed, once the system had settled into a mechanically stable 'jammed' state. The nature of this ensemble has been the focus of many studies [2, 4–6].

Jamming is ubiquitous and occurs in materials of practical importance, such as foams, colloids and grains when they solidify in the absence of thermal fluctuations. Decompressing such a solid to the point where it can no longer achieve mechanical equilibrium leads to unjamming. Studies of the unjamming transition in systems of particles interacting via soft, repulsive potentials have shown that this transition is characterized by power-law scaling of many physical properties [7–12]. However, both the exact nature of the ensemble of jammed states and the unjamming transition remain unclear.

In this letter we report a *direct test* of the Edwards conjecture, using a numerical scheme for computing basin volumes of distinct jammed states (energy minima) of N polydisperse, frictionless disks held at a constant packing fraction ϕ. Uniquely, our numerical scheme allows us to compute Ω, the number of distinct jammed states, and the individual probabilities $p_{i\in\{1,\ldots,\Omega\}}$ of each observed packing to occur. Fig. 1a shows a snapshot of a section of the system, consisting of particles with a hard core and a soft shell. We obtain jammed packings by equilibrating a hard disk fluid and inflating the particles at regular intervals to obtain the desired soft-disk volume fractions (ϕ), followed by energy minimization (see SI). The minimization procedure finds individual stable packings with a probability p_i proportional to the volume v_i of their basin of attraction. Averages computed using this procedure, represented by $\langle\ldots\rangle_{\mathcal{B}}$, would then lead to a bias originating from the different v_i's. Recent advances in numerical methods [13–16]

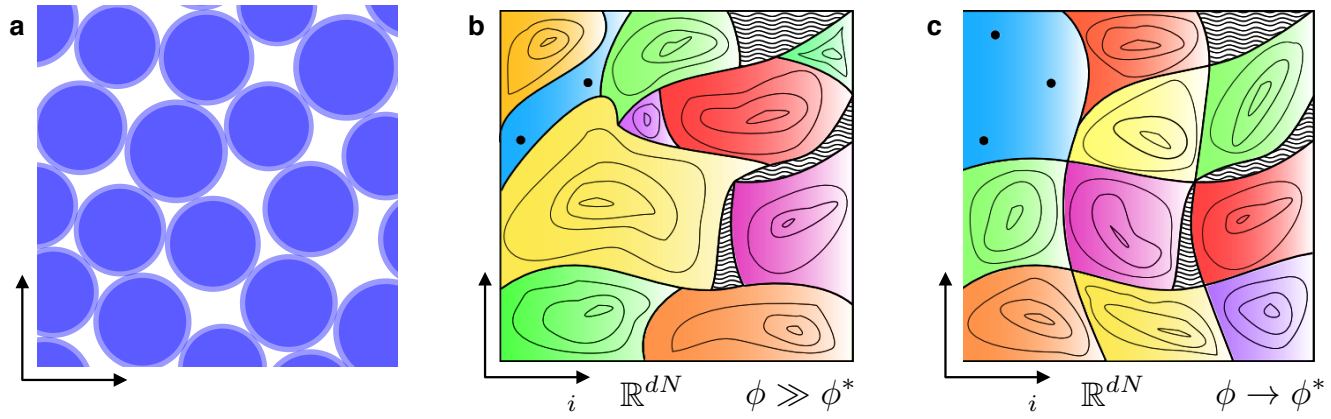

FIG. 1: (a) Snapshot of a jammed packing of disks with a hard core (dark shaded regions) plus soft repulsive corona (light shaded regions). (b)-(c) Illustration of configurational space for jammed packings. The dashed regions are inaccessible due to hard core overlaps. Single coloured regions with contour lines represent the basins of attraction of distinct minima. The dark blue region with solid dots indicates the coexisting unjammed fluid region and hypothetical marginally stable packings, respectively. The volume occupied by the fluid $V_{\rm unj}$ is significant only for finite size systems at or near unjamming. When $\phi \gg \phi^*$ (b) the distribution of basin volumes is broad but as $\phi \to \phi^*$ (c) the distribution of basin volumes approaches a delta function, thus satisfying Edwards' hypothesis.

have now enabled direct computation of v_i, and therefore, an unbiased characterization of the phase space.

We report a detailed analysis of the distribution of v_i or a fixed number of disks $N = 64$ (all maximum system sizes in our study were set by the current limits on computing power). We compute v_i using a thermodynamic integration scheme [13–16], and compute the average basin volume $\langle v\rangle(\phi)$. The number of jammed states is, explicitly, $\Omega(\phi) = V_J(\phi)/\langle v\rangle(\phi)$, where $V_J(\phi)$ is the total available phase space volume at a given ϕ. A convenient way to check equiprobability is to compare the Boltzmann entropy $S_B = \ln\Omega - \ln N!$, which counts all packings with the same weight, and the Gibbs entropy $S_G = -\sum_i^\Omega p_i \ln p_i - \ln N!$. The Gibbs entropy satisfies $S_G \leq S_B$, saturating the bound when all p_i are equal: $p_{i\in\{1,\ldots,\Omega\}} = 1/\Omega$. As shown in Fig. 2a, S_G approaches S_B from below as $\phi \to \phi^*_{N=64} \approx 0.823$. Fig. 1b-c schematically illustrates the evolution of the basin volumes as the packing fraction is reduced.

To characterize the distribution of basin volumes, we analyse the statistics of v_i along with the pressure P_i of each packing. It is convenient to study $F_i \equiv -\ln v_i$ as a function of $\Lambda_i \equiv \ln P_i$. As shown in Fig. 2b, we observe a strong correlation between F_i and Λ_i which can be described by a linear relationship $\langle F\rangle_{\mathcal{B}}(\phi;\Lambda) \propto \lambda(\phi)\Lambda$, where $\langle F\rangle_{\mathcal{B}}(\phi;\Lambda)$ represents the average over all basins at a given Λ. Defining $f = F/N$, this linear relationship [13] can be written as (see SI for details):

$$\begin{aligned}\langle f\rangle_{\mathcal{B}}(\phi;\Lambda) =& \lambda(\phi)\Lambda + c(\phi)\\ =& \lambda(\phi)\Delta\Lambda + \langle f\rangle_{\mathcal{B}}(\phi)\ ,\end{aligned} \tag{1}$$

where $\Delta\Lambda = \Lambda - \langle\Lambda\rangle_{\mathcal{B}}(\phi)$. As can be seen from Fig. 2c-d, within the range of volume fractions studied, $\lambda(\phi)$ and $c(\phi)$ are proportional to $\Delta\phi \equiv \phi - \phi^*_{N=64}$. For Edwards' hypothesis to be satified, while preserving the linear relationship (Eq. 1), λ must necessarily vanish. By extrapolation we find that $\lambda \to 0$ at packing fraction $\phi^*_{N=64} = 0.824 \pm 0.072$, that is precisely where our extrapolation yields $S_G = S_B$, indicating that the vanishing of λ can be used to estimate the point of equiprobability. The fluctuations σ_f^2, σ_Λ^2, and the covariance $\sigma_{f\Lambda}^2$, obtained from the elements of the covariance matrix $\mathbf{\Sigma} = ((\sigma_f^2, \sigma_{f\Lambda}^2), (\sigma_{f\Lambda}^2, \sigma_\Lambda^2))$ of the joint distribution of f and Λ(see SI for details), define λ and c:

$$\begin{aligned}\lambda(\phi) \equiv& \frac{\sigma_{f\Lambda}^2(\phi)}{\sigma_\Lambda^2(\phi)},\\ c(\phi) \equiv& \langle f\rangle_{\mathcal{B}}(\phi) - \frac{\sigma_{f\Lambda}^2(\phi)}{\sigma_\Lambda^2(\phi)}\langle\Lambda\rangle_{\mathcal{B}}(\phi).\end{aligned} \tag{2}$$

From Fig. 2b we observe that as $\lambda \to 0$ at $\phi^*_{N=64}$, σ_Λ^2 increases to a maximum, while σ_f^2 and $\sigma_{f\Lambda}^2$ decrease (see SI). We expect the main features of these distributions to be preserved as the system size N is increased [13], which suggests

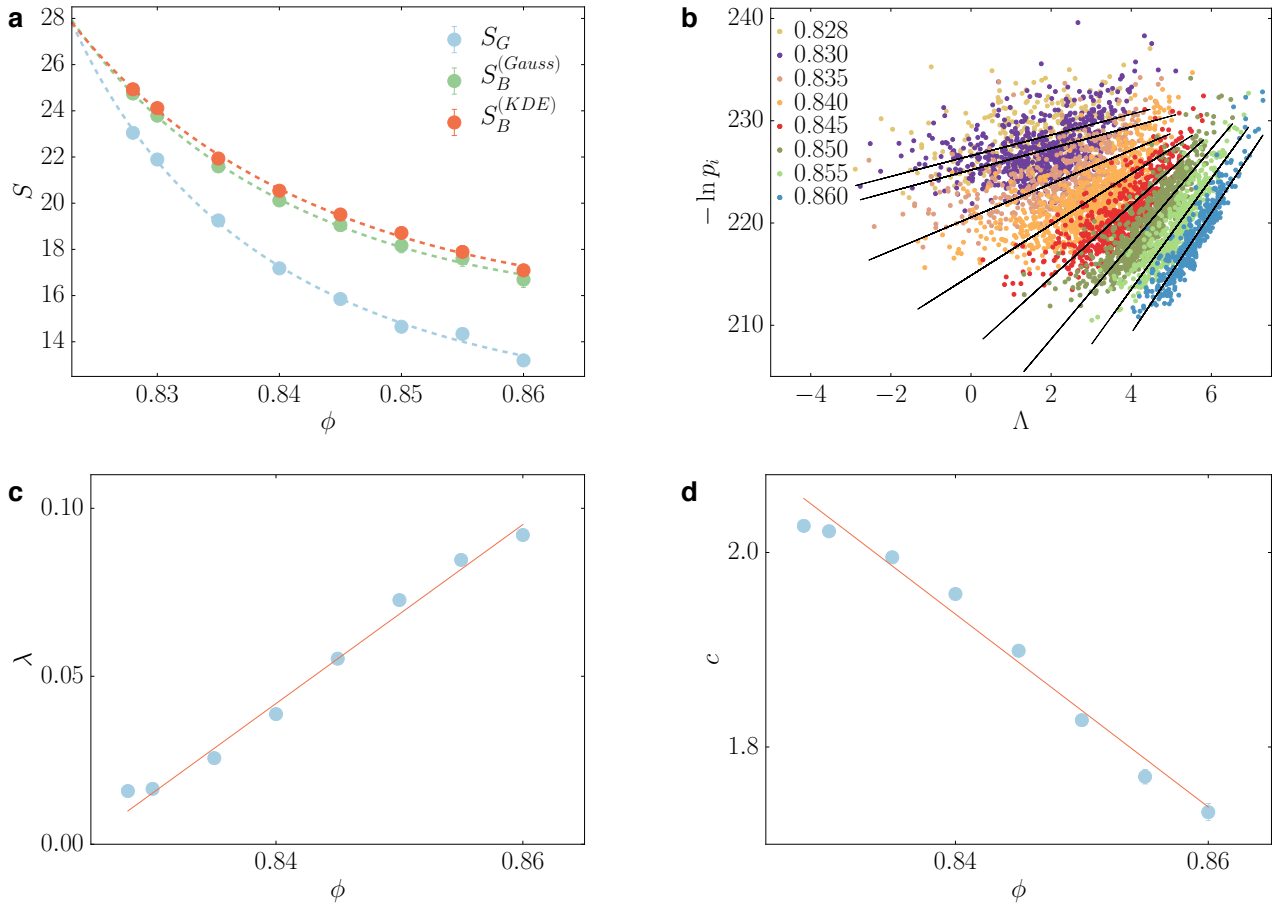

FIG. 2: (a) Gibbs entropy S_G and Boltzmann entropy S_B as a function of volume fraction. S_B is computed both parametrically by fitting $\mathcal{B}(f)$ with a generalised Gaussian function ('Gauss') and non-parametrically by computing a Kernel Density Estimate ('KDE') as in Ref.[13]. Dashed curves are a second order polynomial fit. (b) Scatter plot of the negative log-probability of observing a packing, $-\ln p_i = F_i + \ln V_J(\phi)$, where V_J is the accessible fraction of phase space (see SI) as a function of log-pressure, Λ. Black solid lines are lines of best fit computed by linear minimum mean square error using a robust covariance estimator (see SI). (c) Slopes $\lambda(\phi)$ and (d) intercepts $c(\phi)$ of linear fits for Eq. 1. Solid lines are lines of best fit and error bars refer to the standard error.

that for larger N where an exact computation of v_i and S_B is not feasible, the maximum in σ_Λ^2 can be used to identify ϕ_N^*. We have measured $\chi_\Lambda = N\sigma_\Lambda^2$ using our (biased) sampling scheme for systems upto $N = 128$ (see inset of Fig. 3a) and finite size scaling indicates that χ_Λ diverges as $\phi \to \phi^*_{N\to\infty} = 0.841(3)$ (see SI).

Interestingly, we find evidence that in the thermodynamic limit, the point of equiprobability $\phi^*_{N\to\infty}$, coincides with the point at which the system unjams, $\phi^J_{N\to\infty}$. We use two characteristics of the unjamming transition to locate $\phi^J_{N\to\infty}$ (i) the average pressure of the packings goes to zero, and therefore $\langle\Lambda\rangle \to -\infty$ (see Fig 3b) and (ii) the probability of finding jammed packings, p_J, goes to zero (see inset of Fig 3 b). A scaling analysis indicates that $\langle\Lambda\rangle \to -\infty$ as $\phi^J_{N\to\infty} = 0.841(3)$, and $p_J \to 0$ as $\phi^J_{N\to\infty} = 0.844(2)$ (see SI). We thus find that $\phi^*_{N\to\infty} = \phi^J_{N\to\infty}$ within numerical error and up to corrections to finite size scaling [17]. Our simulations therefore lead to the surprising conclusion that the Edwards conjecture appears to hold precisely at the (un)jamming transition.

Why is χ_Λ related to the unjamming transition? As the particles interact via purely repulsive potentials, P is strictly positive, which implies that the fluctuations of P have a floor and go to zero at unjamming. The *relative* fluctuations $\chi_P \equiv N\sigma^2\,(P/\langle P\rangle_\mathcal{B})$, can be non-zero, and a diverging χ_P would then imply a diverging χ_Λ. Because of the bounded nature of P, however, χ_P can *only* diverge at the unjamming transition where $\langle P\rangle_\mathcal{B} \to 0$ (see SI). We find that χ_P does diverge (Fig. 3 a) and finite size scaling yields $\phi^J_{N\to\infty} = 0.841(3)$ (see SI). Returning to the $N = 64$ case that we have analysed using the basin volume statistics, we find that both χ_P and χ_Λ saturate to their maximum values over similar ranges of ϕ and our estimate $\phi^*_{N=64} = 0.824(70)$ where $S_G = S_B$ and $\lambda \to 0$, falls in this region. In addition, the average number of contacts, $\langle z\rangle_\mathcal{B}(\phi^*_{N=64}) = 4.058 \pm 0.33$: close to the isostatic value

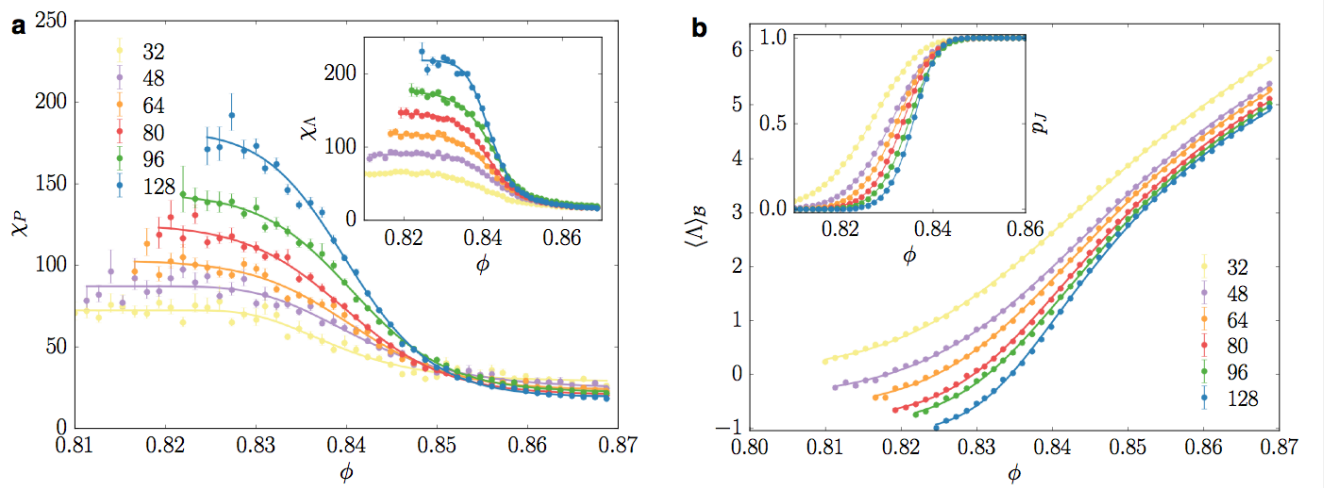

FIG. 3: (a) $\chi_P \equiv N\sigma^2(P/\langle P\rangle_{\mathcal{B}})$ and (inset) $\chi_\Lambda \equiv N\sigma^2_\Lambda$, plotted as a function of volume fraction ϕ. By finite size scaling (see SI) we show that the curves diverge in the thermodynamic limit as $\phi \to \phi^{J/*}$, implying $\phi^*_{N\to\infty} = \phi^J_{N\to\infty} = 0.841(3)$, see main text for discussion. For $\phi \gg \phi^J_N$, χ_P approaches a constant value indicating the absence of correlations far from the transition. (b) Observed average log-pressure $\langle\Lambda\rangle_{\mathcal{B}}$ and (inset) probability of obtaining a jammed packings by our protocol, as a function of volume fraction ϕ. By finite size scaling (see SI) we show that $\langle\Lambda\rangle_{\mathcal{B}} \to -\infty$ as $\phi \to \phi^J_{N\to\infty} = 0.841(3)$ and p_J collapses for $\phi^J_{N\to\infty} = 0.844(2)$, thus locating the unjamming point. Error bars, computed by BCa bootstrap [22], refer to 1σ confidence intervals. Solid lines are generalised sigmoid fits of the form $f(\phi) = a - (a-b)/(1+\exp(-w\Delta\phi))^{1/u}$. We only show values of ϕ where the probability of finding a jammed packing is at least 1%, so that the observables are computed over sufficiently large samples.

$z^{(iso)}_{N=64} \equiv 2d - 2/64 \approx 3.97$ [10] (see SI).

Finally, we note that the states in the generalized Edwards ensemble [5, 18–20] characterized by ϕ and P have basin volumes that are similar, if not identical, over the full range of ϕ that we have explored (see scatter plot in Fig. 2b), indicating that equiprobability in the stress-volume ensemble [5, 18] is a more robust formulation of the Edwards hypothesis. This observation is consistent with recent experiments[21].

In conclusion, we have reported numerical evidence supporting the existence of a flat measure at unjamming for 2D soft repulsive sphere systems. Although, the equiprobability of jammed states at a given packing fraction was posited by Edwards for jammed packings of hard particles, our analysis shows that for soft particles, the Edwards hypothesis is valid only for the marginally jammed state at $\phi^*_{N\to\infty} = \phi^J_{N\to\infty}$, where the jamming probability vanishes, the entropy is maximized, and relative pressure fluctuations diverge. We have shown not only that there exist a practical 'Edwardsian' packing generation protocol, capable of sampling jammed states equiprobably, but we have uncovered an unexpected property of the energy landscape for this class of systems. At this stage we cannot establish whether the same considerations are valid in 3D, although the already proven validity of Eq. 1 in 3D would suggest so [13]. The exact value of the entropy at unjamming, whether finite or not, also needs to be elucidated. The implications for 'soft' structural glasses is apparent: at ϕ^* the uniform size of the basins implies that the system, when thermalised, has the same probability of visiting all of its basins of attraction, hence there are no preferred inherent structures. This could be a signature of the hard-sphere transition occurring at the same point [23]. Our approach can therefore be extended to spin-glasses and related problems, and it would be clearly very exciting to explore the analogies and differences between 'jamming' in various systems for which the configuration space can break up into many distinct basins.

S.M. acknowledges financial support by the Gates Cambridge Scholarship. K.J.S. acknowledges support by the Swiss National Science Foundation under Grant No. P2EZP2-152188 and No. P300P2-161078. D.F. acknowledges support by EPSRC Programme Grant EP/I001352/1 and EPSRC grant EP/I000844/1. K.R. and B.C. acknowledge the support of NSF-DMR 1409093 and the W. M. Keck Foundation.

* sm958@cam.ac.uk

[1] R. Laughlin, *A Different Universe: Reinventing Physics from the Bottom Down*, Basic Books, 2006.
[2] S. F. Edwards and R. B. S. Oakeshott, Physica A **157**, 180–190 (1991).
[3] J. W. Gibbs, *Elementary Principles of Statistical Mechanics*, Charles Scribner's sons, New York, Edward Arnold, London (1902).
[4] S. F. Edwards, and D. V. Grinev, Advances in Physics, 51, 1669 (2010).
[5] D. Bi, S. Henkes, K. E. Daniels, and B. Chakraborty, Annual Review of Condensed Matter Physics, 6,63, (2015).
[6] A. Baule, F. Morone, H. Hermann, and H.A. Makse, arXiv1602.04369 (2016).
[7] P. Olsson and S. Teitel, Phys. Rev. Lett. 99, 178001 (2007).
[8] M. Wyart, S.R. Nagel, and T.A. Witten, EPL 72, 486 (2005).
[9] L. E. Silbert, A. J. Liu and S. R. Nagel, Phys. Rev. E 73 041304 (2006).
[10] C. Goodrich, A. J. Liu, and J. P. Sethna, PNAS, 20160158 (2016).
[11] K. Ramola and B. Chakraborty, arXiv:1604.06148, (2016).
[12] K. Ramola and B. Chakraborty, arXiv:1609.07054, (2016).
[13] S. Martiniani, K. J. Schrenk, J. D. Stevenson, D. J. Wales, D. Frenkel, Phys. Rev. E, 93, 012906 (2016).
[14] N. Xu, D. Frenkel, and A. J. Liu, Phys. Rev. Lett., 106, 245502 (2011).
[15] D. Asenjo and F. Paillusson and D. Frenkel, 112, 098002 (2014).
[16] S. Martiniani, K. J. Schrenk, J. D. Stevenson, D. J. Wales, D. Frenkel, Phys. Rev. E 94, 031301(R) (2016).
[17] D. Vagberg, D. Valdez-Balderas, M. A. Moore., P. Olsson, S. Teitel, Physical Review E, 83(3), 030303 (2011).
[18] R. Blumenfeld, and S. F. Edwards, J. Phys. Chem. B, 113, 3981 (2009).
[19] S. Henkes, C. S. O'Hern, and B. Chakraborty, Phys. Rev. Lett., 99, 038002 (2007).
[20] S. Henkes, and B. Chakraborty, Phys. Rev. E., 79, 061301 (2009).
[21] J. G. Puckett, and K. E. Daniels, Phys. Rev. Lett., 110, 058001 (2013).
[22] B. Efron, J. Am. Stat. Assoc. 82, 397 (1987).
[23] P. Charbonneau, J. Kurchan, G. Parisi, P. Urbani, F. Zamponi arXiv:1605.03008 (2016).

Supplementary Information: Are some packings more equal than others? A direct test of the Edwards conjecture

Stefano Martiniani,[1,*] K. Julian Schrenk,[1] Kabir Ramola,[2] Bulbul Chakraborty,[2] and Daan Frenkel[1]

[1] *Department of Chemistry, University of Cambridge, Lensfield Road, Cambridge, CB2 1EW, UK*

[2] *Martin Fisher School of Physics, Brandeis University, Waltham, MA 02454, USA*

arXiv:1610.06328v1 [cond-mat.soft] 20 Oct 2016

PACKING PREPARATION PROTOCOL

In this section we describe the algorithm that we have used to sample the phase space of jammed packings. This procedure samples each configuration proportional to the volume of its basin of attraction.

Hard sphere fluid sampling

We start by equilibrating a fluid of N hard disks (that serve as the cores of the particles with soft outer shells) at a volume fraction ϕ_{HS} in a square box with periodic boundary conditions. The particle radii are sampled from a truncated Gaussian distribution with mean $\mu = 1$ and standard deviation $\sigma = 0.1$. We achieve equilibration by performing standard Markov Chain Monte Carlo (MCMC) simulations consisting of single particle displacements and particle-particle swaps, as in [1]. To assure statistical independence, we draw fluid configurations every n_{MC} steps, where n_{MC} is (pre-computed by averaging over multiple simulations) the total number of MCMC steps necessary for each individual particle to diffuse at least a distance equal to the largest diameter in the system.

Soft shells and minimization

We next take each equilibrated hard disk fluid configuration and inflate the particles (instantaneously) with a WCA-like soft outer shell [2], to reach the target soft packing fraction $\phi_{\rm SS} > \phi_{\rm HS}$. Each hard sphere is inflated proportionally to its radius, so that the soft sphere radius is given by

$$r_{\rm SS} = \left(\frac{\phi_{\rm SS}}{\phi_{\rm HS}}\right)^{1/d} r_{\rm HS}, \tag{S1}$$

where d is the dimensionality of the box (2 in our case), and $r_{\rm SS}$ and $r_{\rm HS}$ are the soft and hard sphere radii respectively. Clearly, this procedure does not change the polydispersity of the sample. The radii are identical across volume fractions and system sizes, and the hard disk fluid density is chosen so that the radius ratio of hard to soft disks is $(0.88/0.7)^{1/2} \approx 1.121$.

Next, particle inflation is followed by energy minimization using FIRE [3, 4], to produce mechanically stable packings at the desired soft volume fractions ϕ. This protocol has the advantage of generating packings sampled proportionally to the volume of their basin of attraction. In our simulations, we considered all mechanically stable packings, irrespective of the number of 'rattlers'. To guarantee mechanical stability we required that the total number of contacts is sufficient for the bulk modulus to be strictly positive, $N_{\rm min} = d(N_{nr} - 1) + 1$ [5], where N_{nr} is the number of non-rattlers and d the dimensionality of the system.

HS-WCA POTENTIAL

We define the WCA-like potential around a hard core as follows: consider two spherical particles with a distance between the hard cores $r_{\rm HS}$, implying a soft core contact distance $r_{\rm SS} = r_{\rm HS}(1 + \theta)$, with $\theta = (\phi_{\rm SS}/\phi_{\rm HS})^{1/d} - 1$. We

can then write a horizontally shifted hard-sphere plus WCA (HS-WCA) potential as

$$u_{\text{HS-WCA}}(r) = \begin{cases} \infty & r \le r_{\text{HS}}, \\ 4\epsilon \left[\left(\dfrac{\sigma(r_{\text{HS}})}{r^2 - r_{\text{HS}}^2} \right)^{12} \right. & \\ \left. - \left(\dfrac{\sigma(r_{\text{HS}})}{r^2 - r_{\text{HS}}^2} \right)^{6} \right] + \epsilon & r_{\text{HS}} < r < r_{\text{SS}}, \\ 0 & r \ge r_{\text{SS}} \end{cases} \tag{S2}$$

where $\sigma(r_{\text{HS}}) = (2\theta + \theta^2) r_{\text{HS}}^2 / 2^{1/6}$ guarantees that the potential goes to zero at r_{SS}. For computational convenience (avoidance of square-root evaluations), the potential in Eq. S2 differs from the WCA form in that the inter-particle distance in the denominator of the WCA potential has been replaced with a difference of squares.

We numerically evaluate this potential, matching the gradient and linearly continuing the function $v_{\text{HS-WCA}}(r)$ for $r \le r_{\text{HS}} + \varepsilon$, where $\varepsilon > 0$ is an arbitrary small constant, such that minimization is still meaningful if hard core overlaps do occur.

TOTAL ACCESSIBLE VOLUME

The basins of attraction of energy minima tile the "accessible" phase space (schematically shown in Fig. 1b-c of the main text). This inaccessible part of the phase space arises due to hard core constraints and the existence of fluid states (see e.g. [1]). The total phase space volume is equal to V_{box}^N. The inaccessible part of this volume arising from the hard core constraints (shown as hatched areas in Fig. 1 of main text) is denoted by V_{HS}, and the part corresponding to the coexisting unjammed fluid states is denoted by V_{unj} (shown as blue regions with squares in Fig. 1 of main text). V_{unj} is significant only for finite size systems at or near unjamming. We denote the space tiled by the basins of mechanically stable jammed packings by V_J. We then have $V_J = V_{\text{box}}^N - V_{\text{HS}} - V_{\text{unj}}$. In practice we compute V_J using the following equation

$$\ln V_J(N, \phi_{\text{HS}}, \phi_{\text{SS}}) = N \ln V_{\text{box}} - N f_{\text{ex}}(\phi_{\text{HS}}) + \ln p_J(\phi_{\text{SS}}), \tag{S3}$$

where $f_{\text{ex}}(\phi_{\text{HS}})$ is the excess free energy, *i.e.* the difference in free energy between the hard sphere fluid and the ideal gas, computed from the Santos-Yuste-Haro (eSYH) equation of state [6] as in [1], and $p_J(\phi_{\text{SS}})$ is the probability of obtaining a jammed packing at soft volume fraction ϕ_{SS} with our protocol, shown in Fig. S5.

We can then define the probability of sampling the i-th packing as $p_i = v_i / V_J$, where v_i is the volume of the basin of attraction of the packing. The total number of jammed packings is given by $\Omega = V_J / \langle v \rangle$, where $\langle v \rangle$ is the unbiased average basin volume. Details of the computation of v_i are discussed in Refs.[1, 7].

POWER-LAW BETWEEN PRESSURE AND BASIN VOLUME

A power-law relationship between the volume of the basin of attraction of a jammed packing and its pressure was first reported in [1]. In what follows we provide insight into this expression on the basis of this work's findings. We observe that distributions of negative basin log-volumes, $F = -\ln v_{\text{basin}}$, and log-pressures, $\Lambda = \ln P$, are approximately normally distributed (see Fig. S1 and S6). We therefore expect their joint probability to be well-approximated by a bivariate Gaussian distribution $\mathcal{B}(\phi; F, \Lambda) = \mathcal{N}(\mu, \mathbf{\Sigma})$ [23], with mean $\mu = (\mu_F, \mu_\Lambda)$ and covariance matrix $\mathbf{\Sigma} = ((\sigma_F^2, \sigma_{F\Lambda}^2), (\sigma_{F\Lambda}^2, \sigma_\Lambda^2))$ [8]. This is consistent with the elliptical distribution of points in Fig. 2b of the main text. For a given random variable X, with an (observed/biased) marginal distribution $\mathcal{B}(X)$, the mean is given by $\mu_X(\phi) = \langle X \rangle_{\mathcal{B}} = \int X \mathcal{B}(\phi; X)\, \mathrm{d}X$. Similarly, the (biased) conditional expectation of F for a given Λ is then [8]

$$\langle F \rangle_{\mathcal{B}(\mathbf{\Gamma})}(\phi; \Lambda) \equiv \mathbb{E}[F|\phi; \Lambda] = \frac{\sigma_{F\Lambda}^2(\phi)}{\sigma_\Lambda^2(\phi)} (\Lambda - \mu_\Lambda(\phi)) + \mu_F(\phi). \tag{S4}$$

This is simply the linear minimum mean square error (MMSE) regression estimator for F, i.e. the linear estimator $\hat{Y}(X) = aX + b$ that minimizes $\mathbb{E}[(Y - \hat{Y}(X))^2]$. The expectation of the dimensionless free energy $\langle F \rangle_{\mathcal{B}(\mathbf{\Gamma})}(\phi; \Lambda) = -\langle \ln v \rangle_{\mathcal{B}(\mathbf{\Gamma})}(\phi; \Lambda) \ge -\ln \langle v \rangle_{\mathcal{B}(\mathbf{\Gamma})}(\phi; \Lambda)$ [9] is the average negative basin log-volume at volume fraction ϕ and log-pressure Λ. Here the average is also taken over all other relevant, but unknown, order parameters $\mathbf{\Gamma}$, such that

$\langle F\rangle_{\mathcal{B}(\mathbf{\Gamma})}(\phi;\Lambda) = \int \mathrm{d}\mathbf{\Gamma}\mathcal{B}(\mathbf{\Gamma})F(\phi;\mathbf{\Gamma},\Lambda)$. In other words, we write the expectation of F at a given pressure as the (biased) average over the unspecified order parameters $\mathbf{\Gamma}$. An example of such a parameter would be some topological variable that makes certain topologies more probable than others. Note that $F(\phi,\Lambda;\Gamma)$ is narrowly distributed around $\mathbb{E}[F|\phi;\Lambda]$. To simplify the notation we write $\langle F\rangle_{\mathcal{B}(\mathbf{\Gamma})}(\phi;\Lambda) \equiv \langle F\rangle_{\mathcal{B}}(\phi;\Lambda)$. We can thus rewrite the power-law reported in [1] as

$$\begin{aligned}\langle f\rangle_{\mathcal{B}}(\phi;\Lambda) =&\lambda(\phi)\Lambda + c(\phi)\\ =&\frac{\sigma^2_{f\Lambda}(\phi)}{\sigma^2_{\Lambda}(\phi)}\Lambda - \frac{\sigma^2_{f\Lambda}(\phi)}{\sigma^2_{\Lambda}(\phi)}\mu_{\Lambda}(\phi) + \mu_f(\phi)\\ =&\frac{\sigma^2_{f\Lambda}(\phi)}{\sigma^2_{\Lambda}(\phi)}\Delta\Lambda + \mu_f(\phi)\end{aligned} \tag{S5}$$

where $f = F/N$ is the basin log-volume per particle and $\lambda \equiv 1/\kappa$ is the slope of the power-law relation, which depends crucially on the packing fraction ϕ. The last equality in Eq. S5 highlights how $\lambda(\phi)$ controls the contributions of the fluctuations of the log-pressures $\Delta\Lambda \equiv \Lambda - \mu_{\Lambda}(\phi)$ to changes in the basin log-volume. Note that one can rewrite the ratio of fluctuations as $\sigma^2_{f\Lambda}/\sigma^2_{\Lambda} = \rho_{f\Lambda}\sigma_f/\sigma_{\Lambda}$ where $\rho_{f\Lambda} = \sigma^2_{f\Lambda}/(\sigma_f\sigma_{\Lambda})$ is the linear correlation coefficient of f and Λ. Finally, we can gain further insight into the power-law dependence by noting that

$$\lambda(\phi) \equiv \frac{\sigma^2_{f\Lambda}(\phi)}{\sigma^2_{\Lambda}(\phi)} \tag{S6}$$

$$c(\phi) \equiv \mu_f(\phi) - \frac{\sigma^2_{f\Lambda}(\phi)}{\sigma^2_{\Lambda}(\phi)}\mu_{\Lambda}(\phi) \tag{S7}$$

VARIANCE OF RELATIVE PRESSURES

In this section we relate the statistics of the log-pressures of the packings to the *relative* pressures. For a given N and ϕ, with the set of pressures $\{P_i\}$, the log-pressures are given by $\Lambda_i = \ln P_i$ and the relative pressures are $P_i/\langle P\rangle$. The two quantities are then simply related as

$$\ln\left(\frac{P_i}{\langle P\rangle}\right) = \ln P_i - \ln\langle P\rangle = \Lambda_i - \ln\langle P\rangle. \tag{S8}$$

Using Jensen's inequality, we have the following bound for the first moment of the log-pressures

$$\langle\Lambda\rangle = \langle\ln P\rangle \leq \ln\langle P\rangle. \tag{S9}$$

Therefore $\langle P\rangle \to 0$ implies $\langle\Lambda\rangle \to -\infty$. In order to relate the means and the variances of P_i and $\Lambda_i = \ln P_i$, we perform the Taylor expansion

$$\ln P = \ln\langle P\rangle + \left.\frac{d\ln P}{dP}\right|_{P=\langle P\rangle}(P - \langle P\rangle) + ... \tag{S10}$$

We next compute the moments to leading order

$$\begin{aligned}\langle\ln P\rangle &\approx \ln\langle P\rangle,\\ \sigma^2(\ln P) &\approx \frac{\sigma^2(P)}{\langle P\rangle^2} = \sigma^2\left(\frac{P}{\langle P\rangle}\right).\end{aligned} \tag{S11}$$

Thus, to first order, the variance of the log-pressures is equal to the variance of the relative pressures.

Diverging χ_P

For a fixed N and ϕ, the pressures of the individual packings are bounded as

$$0 < P_{\min} \leq P_i \leq P_{\max}. \tag{S12}$$

where $P_{\max}$ and $P_{\min}$ are determined by the packing fraction ϕ, independent of system size, and are physically set limits. We can therefore use Popoviciu's inequality on variances, yielding

$$\sigma^2(P) \leq \frac{1}{4}\left(P_{\max} - P_{\min}\right)^2, \tag{S13}$$

which is also bounded. The relative pressure fluctuations are therefore bounded as

$$\sigma^2\left(\frac{P}{\langle P\rangle}\right) \leq \frac{1}{4}\frac{\left(P_{\max} - P_{\min}\right)^2}{\langle P\rangle^2}. \tag{S14}$$

We thus find that the variance of the relative pressures $\sigma^2\left(\frac{P}{\langle P\rangle}\right)$ can diverge only when $\langle P\rangle \to 0$, which is precisely where the unjamming transition occurs.

DATA ANALYSIS

Reduced units

While presenting data from our computations, we express pressure and volume in reduced units as P/P^* and v/v^* respectively. The unit of volume is given by $v^* \equiv \pi\langle r_{HS}^2\rangle$, where $\langle r_{HS}^2\rangle$ is the mean squared hard sphere radius. The unit of pressure is then $P^* \equiv \epsilon/v^*$, where ϵ is the stiffness of the soft-sphere potential, defined in Eq. S2. The pressure is computed as $P = \mathrm{Tr}(\Sigma)/2V_{\mathrm{box}}$ where Σ is the Virial stress tensor and V_{box} the volume of the enclosing box.

Summary of calculations

For the basin volume calculations we consider systems of $N = 64$ disks sampled at a range of 8 volume fractions $0.828 \leq \phi \leq 0.86$ and for each ϕ we measure the basin volume for about $325 < M < 770$ samples.

For the finite size scaling analysis of the relative pressure fluctuations we study system sizes $N = 32, 48, 64, 80, 96, 128$ for 48 volume fractions in the range $0.81 \leq \phi \leq 0.87$. For each system size we generate up to 10^5 hard disk fluid configurations and compute the pressure for between approximately 10^3 and 10^4 jammed packings (depending on the probability of obtaining a jammed packing at each volume fraction).

Simulations were performed using the open source libraries PELE [10] and MCPELE [11].

Outlier detection and robust covariance estimation

Before manipulating the raw data we remove outliers from the joint distribution $\mathcal{B}(f, \Lambda)$ following the distance-based outlier removal method introduced by Knorr and Ng [12]. This is applied in turn to each dimension, such that we choose to keep only those points for which at least $R = 0.5$ of the remaining data set is within $D = 4\sigma$ (compared to the much stricter $R = 0.9988$, $D = 0.13\sigma$ required to exclude any points further than $|\mu - 3\sigma|$ for normally distributed data [12]). On our datasets we find that this procedure removes typically none and at most 0.5% of all data points.

Mean and covariance estimates of $\mathcal{B}(f, \Lambda)$ are computed using a robust covariance estimator, namely the Minimum Covariance Determinant (MCD) estimator [13, 14] with support fraction $h/n_{\mathrm{samples}} = 0.99$. The MCD estimator defines μ_{MCD}, the mean of the h observations for which the determinant of the covariance matrix is minimal, and Σ_{MCD}, the corresponding covariance matrix [15]. We use these robust estimates of the location and of the covariance matrix to fit our observations by linear MMSE [8], see Fig.2 of the main text.

Before fitting $\mathcal{B}(f)$ (required to compute Ω), we perform an additional step of outlier detection based on an elliptic (Gaussian) envelope criterion constructed using the MCD estimator. We assume a support fraction $h/n_{\mathrm{samples}} = 0.99$ and a contamination equal to 10% [14]. We compute S_G and S_B from the resulting datasets. The procedure is strictly unsupervised and allows us to achieve robust fits despite the small sample sizes. We fit $\mathcal{B}(f)$ using both a (parametric) generalised Gaussian model [16] and a (non-parametric) kernel density estimate (KDE) with Gaussian kernels [14, 17] and bandwidth selection performed by cross validation [1, 18].

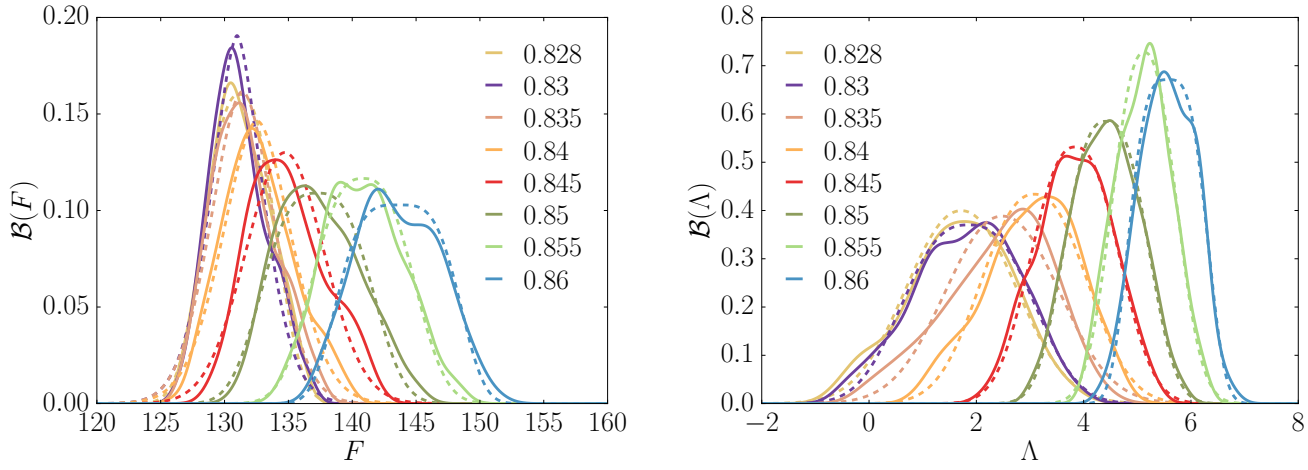

(a) (b)

FIG. S1: Observed distribution of the basin log-volume F (a) and log-pressure Λ (b) for jammed packings of $N = 64$ HS-WCA polydisperse disks at various volume fractions $0.828 \leq \phi \leq 0.86$. Solid lines are Kernel Density Estimates and dashed lines are generalised Gaussian fits.

Error analysis

Errors were computed analytically where possible and propagated using the 'uncertainties' Python package [19]. Alternatively, intervals of confidence were computed by BCa bootstrap [20] using the 'scikit-bootstrap' Python package [21].

RESULTS

Distributions of F and Λ

In Fig. S1 we show the biased distributions $\mathcal{B}(F)$ and $\mathcal{B}(\Lambda)$ of the basin log-volumes and log-pressure, which are the marginal distributions of the joint distribution $\mathcal{B}(F, \Lambda)$ shown in Fig. 2. In Fig. S2 we plot the moments of $\mathcal{B}(F, \Lambda)$, namely the elements of the mean $\mu = (\mu_f, \mu_\Lambda)$ and the elements of the covariance matrix $\mathbf{\Sigma} = ((\sigma_f^2, \sigma_{f\Lambda}^2), (\sigma_{f\Lambda}^2, \sigma_\Lambda^2))$, as well as the linear correlation coefficient $\rho_{f\Lambda} = \sigma_{f\Lambda}^2/(\sigma_f \sigma_\Lambda)$.

Estimates of the equiprobability density $\phi^*_{N=64}$

We summarise the estimated values for $\phi^*_{N=64}$ in Table S1

	λ	$S_B^{(Gauss)}$	$S_B^{(KDE)}$
$\phi^*_{N=64}$	0.824 ± 0.073	0.823	0.823
$\langle z \rangle_{\mathrm{spl}}(\phi^*_{N=64})$	4.058 ± 0.33	4.052	4.052

TABLE S1: Predicted values of $\phi^*_{N=64}$ obtained from the linear extrapolation of $\lambda \to 0$ and from the point of intersection of the Gibbs entropy S_G with the Boltzmann entropy S_B, computed both parametrically by fitting $\mathcal{B}(f)$ with a generalised Gaussian function ('Gauss') and non-parametrically by computing a Kernel Density Estimate ('KDE') of the distribution. The corresponding average contact number has been computed using a spline interpolation of the data in Fig. S3.

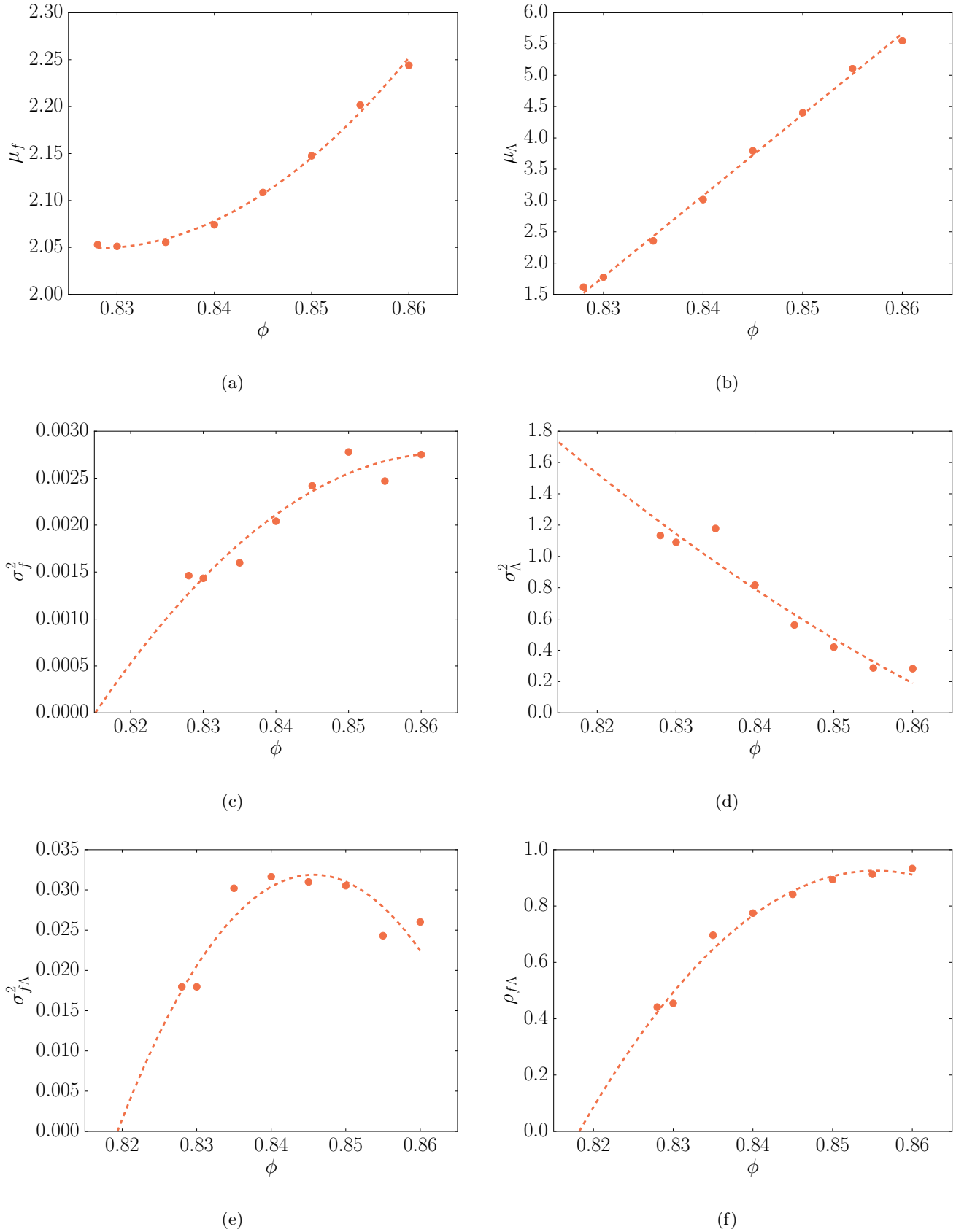

FIG. S2: Moments of the joint distribution $\mathcal{B}(f, \Lambda)$ for jammed packings of $N = 64$ HS-WCA polydisperse disks at various volume fractions $0.828 \leq \phi \leq 0.86$. Elements of the mean $\mu = (\mu_f, \mu_\Lambda)$ are shown in (a) and (b) respectively. Elements of the covariance matrix $\mathbf{\Sigma} = ((\sigma_f^2, \sigma_{f\Lambda}^2), (\sigma_{f\Lambda}^2, \sigma_\Lambda^2))$ are shown in (c)-(e). The linear correlation coefficient $\rho_{f\Lambda} = \sigma_{f\Lambda}^2/(\sigma_f \sigma_\Lambda)$ is shown in (f). Dashed lines are second order polynomial fits and are a guide to the eye, note that for σ_Λ^2 we know from Fig. 3a in main text that the function is sigmoidal and not a monotonically increasing function as suggested by the polinomial fit.

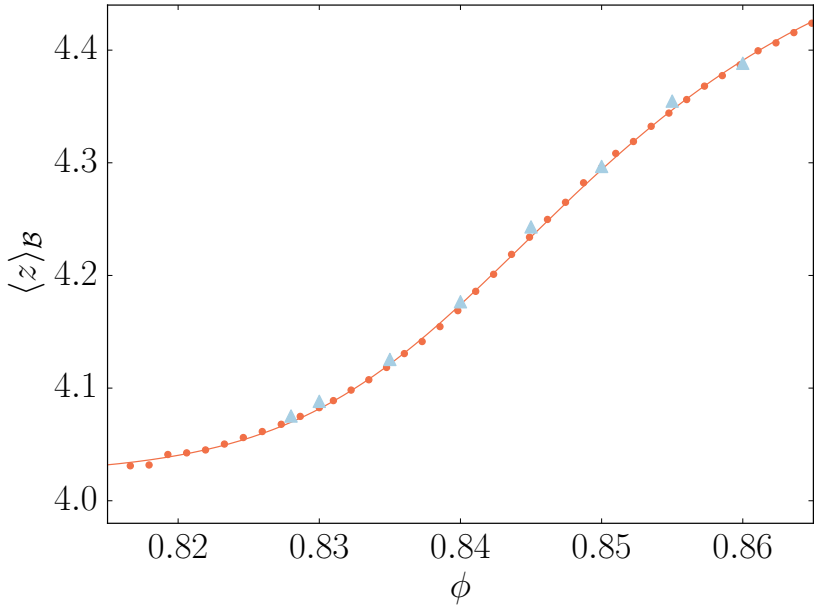

FIG. S3: Observed average contact number for jammed packings of $N = 64$ HS-WCA polydisperse disks. Triangles are estimates from the basin volume measurements datasets. Circles are estimates from the independent measurements used for the finite size scaling analysis. The solid line is a generalised sigmoid fit, Eq. S15, of the latter.

Contact number

The mean contact number is plotted as a function of volume fraction in Fig. S3. The data are fitted with a generalised sigmoid function of the form

$$f(a, b, \phi_0, u, w; \phi) = a - \frac{a - b}{(1 + e^{-w(\phi - \phi_0)})^{1/u}} \tag{S15}$$

In Fig. S4 we also show the fraction of rattlers at different packing fractions for $N = 64$ disks. We note that the fraction of rattlers is maximal and saturates over the same range of densities as where the relative pressure fluctuations are maximal and saturate (see Fig. 3 of main text and finite size scaling section for further discussion).

Finite size scaling

In order to locate the unjamming transition, we compute the probability of obtaining jammed packings as a function of volume fraction ϕ. A finite size scaling collapse for p_J, shown in Fig. S5, yields critical exponents $\nu \approx 1$, $\beta = 0$ and critical volume fraction $\phi^J_{N\to\infty} = 0.844(2)$, in agreement with Vagberg et al. [22]. We obtain an independent estimate of the unjamming transition by locating the point where the average pressure goes to zero and therefore $\langle \Lambda \rangle_{\mathcal{B}} \to -\infty$. KDE distributions for Λ are shown in Fig. S6. The average log-pressure is shown in Fig. S7a and a finite size scaling collapse, Fig. S7b, yields $\nu = 0.50(5)$, $\xi = 0.62(3)$ and critical volume fraction $\phi^J_{N\to\infty} = 0.841(3)$.

We then analyse the relative pressure fluctuations $\chi_P = N\sigma^2(P/\langle P \rangle_{\mathcal{B}})$ and the log-pressure fluctuations $\chi_\Lambda = N\sigma^2_\Lambda$. A scaling collapse for different system sizes of $\chi_P L^{-\gamma/\nu}$ vs. $L^{1/\nu}\left(\phi/\phi^J_{N\to\infty} - 1\right)$ with $L = N^{1/d}$, shown in Fig. S8a, yields $\nu = 0.5(3)$, $\gamma = 0.47(5)$ and $\phi^J_{N\to\infty} = 0.841(3)$. An analogous scaling collapse of $\chi_\Lambda L^{-\gamma/\nu}$ vs. $L^{1/\nu}\left(\phi/\phi^*_{N\to\infty} - 1\right)$, shown in Fig. S8b, yields $\nu = 0.5(3)$, $\gamma = 0.89(5)$ and $\phi^*_{N\to\infty} = 0.841(3)$.

Together these results leads us to conclude that the point of equiprobability $\phi^*_{N\to\infty}$ coincides with the unjamming point $\phi^J_{N\to\infty}$, to within numerical error and finite size corrections that we do not take into account. Note that the precise numerical value of ν varies through the literature and has been shown to depend on the quantity being observed, and also crucially on finite size corrections to scaling [22]. In this work we have not attempted to establish ν definitely, nor elucidate its origin with respect to the diverging correlation length(s) that might be involved.

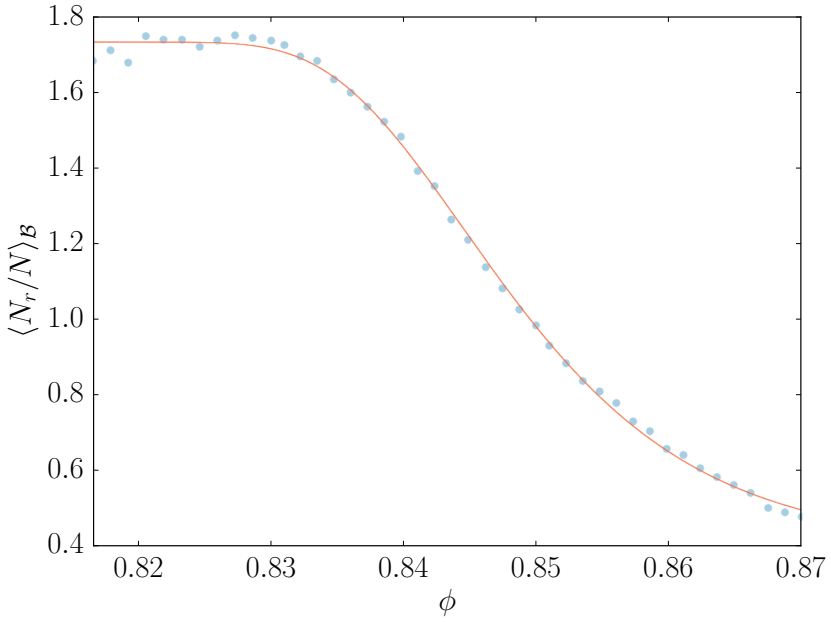

FIG. S4: Fraction of rattlers for jammed packings of $N = 64$ HS-WCA polydisperse disks. We find this tends to a maximum and saturates over the same range of packing fractions where relative pressure fluctuations are maximal, see Fig. 3 of main text. The solid line is a generalised sigmoid fit, Eq. S15.

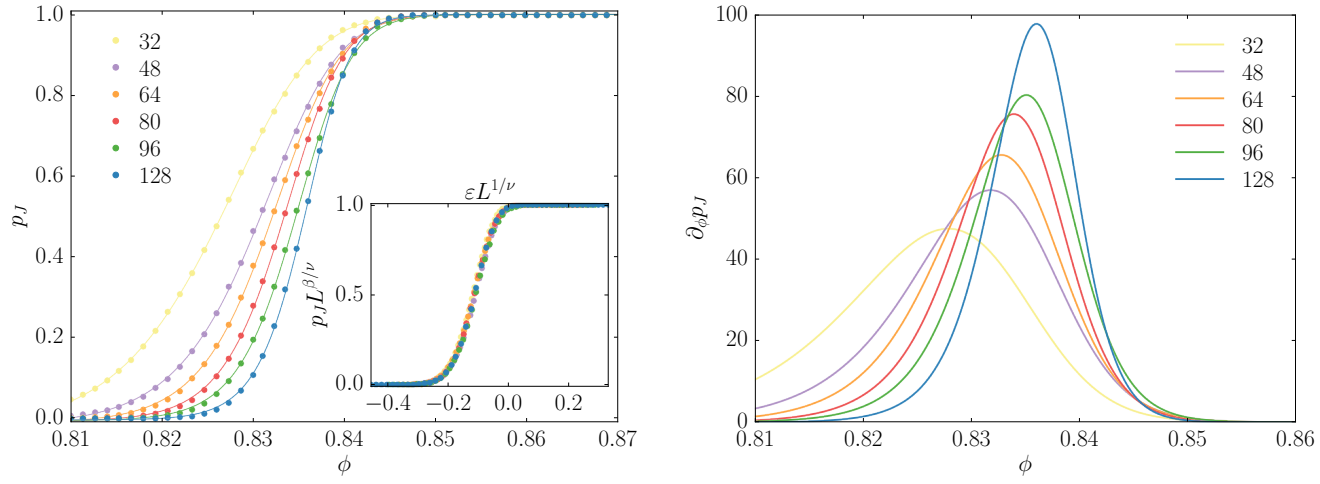

(a) (b)

FIG. S5: (a) Probability of obtaining a jammed packing p_J by our preparation protocol for $N = 32$ to 128 HS-WCA polydisperse disks as a function of volume fraction. Inset: Scaling collapse for $p_J L^{\beta/\nu}$ vs. $L^{1/\nu}\left(\phi/\phi^J_{N\to\infty} - 1\right)$, with $L = N^{1/d}$, yields critical exponents $\nu \approx 1$, $\beta = 0$ and critical volume fraction $\phi^J_{N\to\infty} = 0.844(2)$. Circles are observed data and solid lines correspond to sigmoid fits, Eq. S15. (b) Derivative of the sigmoid fits for p_J for different numbers of disks.

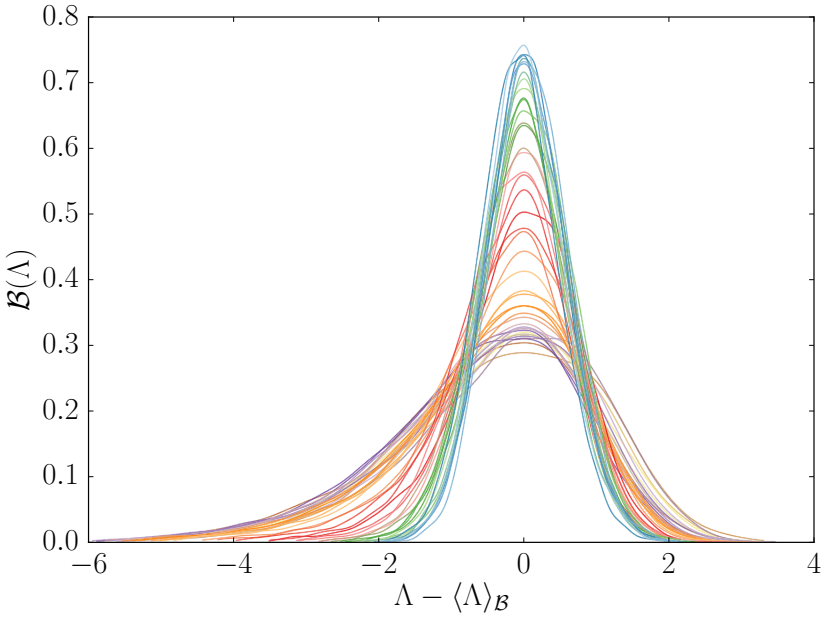

FIG. S6: Log-transformed observed (biased) distribution of pressures for jammed packings of $N = 64$ HS-WCA polydisperse disks, centred around the mean. The variance grows for decreasing volume fractions and becomes more skewed towards low pressures. The overall Gaussian shape is consistent with a log-normal distribution of pressures.

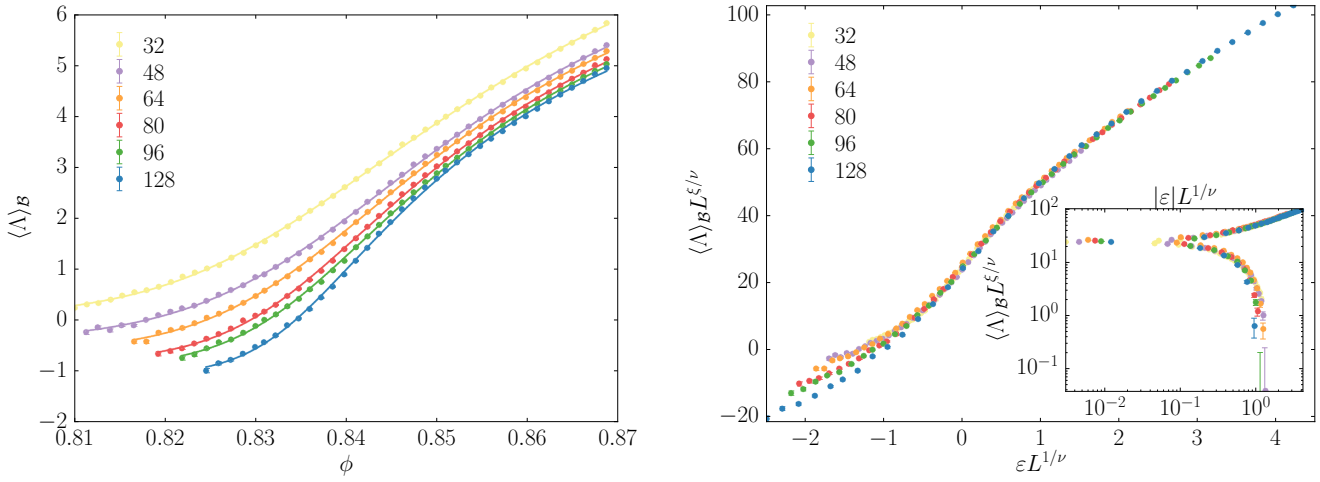

(a) (b)

FIG. S7: (a) Average log-pressure $\langle\Lambda\rangle_{\mathcal{B}}$ for N HS-WCA polydisperse disks. (b) Scaling collapse for $\langle\Lambda\rangle_{\mathcal{B}}L^{\xi/\nu}$ vs. $L^{1/\nu}\left(\phi/\phi^{J}_{N\to\infty} - 1\right)$, with $L = N^{1/d}$. The estimated critical exponents are $\nu = 0.50(5)$ and $\xi = 0.62(3)$, and the critical volume fraction $\phi^{J}_{N\to\infty} = 0.841(3)$. Inset: A logarithmic plot of the same data. Circles are observed data and solid lines are sigmoid fits, Eq. S15. Error bars, computed by BCa bootstrap [20], refer to 1σ confidence intervals.

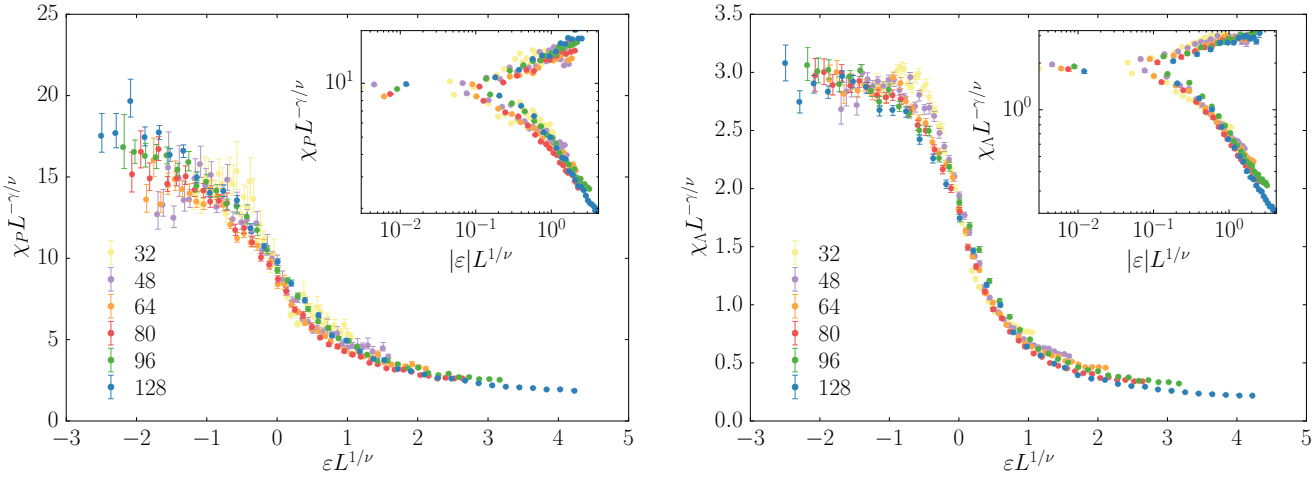

(a) (b)

FIG. S8: (a) Data collapse from finite size scaling analysis of the variance of the relative pressures. The plot shows $\chi_P L^{-\gamma/\nu}$ vs. $L^{1/\nu}\left(\phi/\phi^J_{N\to\infty} - 1\right)$, with $L = N^{1/d}$. The estimated critical exponents are $\nu = 0.50(3)$ and $\gamma = 0.47(5)$, and the critical volume fraction is $\phi^J_{N\to\infty} = 0.841(3)$. (b) Scaling collapse of the variance of the log-pressures. The plot shows $\chi_\Lambda L^{-\gamma/\nu}$ vs. $L^{1/\nu}\left(\phi/\phi^*_{N\to\infty} - 1\right)$. The estimated critical exponents are $\nu = 0.5(3)$ and $\gamma = 0.89(5)$, and the critical volume fraction is $\phi^*_{N\to\infty} = 0.841(3)$. Error bars, computed by BCa bootstrap [20], refer to 1σ confidence intervals.

* sm958@cam.ac.uk

[1] S. Martiniani, K. J. Schrenk, J. D. Stevenson, D. J. Wales, D. Frenkel, Phys. Rev. E, 93, 012906 (2016).
[2] J. D. Weeks and D. Chandler, H. C. Andersen, J. Chem. Phys., 54, 12, 5237 (1971).
[3] E. Bitzek, P. Koskinen, F. Ghler, M. Moseler, P. Gumbsch, Phys. Rev. Lett., 97, 170201 (2006).
[4] D. Asenjo, J. D. Stevenson, D. J. Wales, D. Frenkel, J. Chem. Phys. B, 117(42), 1271 (2013).
[5] C. P. Goodrich, A. J. Liu, and S. R. Nagel, Phys. Rev. Lett. 109, 95704 (2012).
[6] A. Santos, S. B. Yuste, and M. Lopez De Haro, Mol. Phys. 96, 1 (1999).
[7] S. Martiniani, K. J. Schrenk, J. D. Stevenson, D. J. Wales, D. Frenkel, Phys. Rev. E 94, 031301(R) (2016).
[8] D. P. Bertsekas, J. N. Tsitsiklis. Introduction to probability. Vol. 1. Belmont, MA: Athena Scientific, 2002.
[9] E. W. Weisstein, "Jensen's Inequality." From MathWorld – A Wolfram Web Resource.
[10] https://github.com/pele-python/pele
[11] https://github.com/pele-python/mcpele
[12] E. M. Knorr, R. T. Ng, Proceedings of the International Conference on Very Large Data Bases (1998).
[13] P. J. Rousseeuw, and K. Van Driessen, Technometrics 41, 3 (1999)
[14] Pedregosa et al., J. Mach. Lern. Res. 12, 2825 (2011).
[15] M. Hubert, M. Debruyne, Wiley interdisciplinary reviews: Computational statistics, 2(1), 36 (2010).
[16] S. Nadarajah, J. Appl. Stat. 32, 7, 685 (2005).
[17] C. M. Bishop, Pattern Recognition and Machine Learning (Springer, New York, 2009).
[18] A. W. Bowman, Biometrika 71, 353 (1984.)
[19] https://github.com/lebigot/uncertainties
[20] B. Efron, J. Am. Stat. Assoc. 82, 397 (1987).
[21] https://github.com/cgevans/scikits-bootstrap
[22] D. Vagberg, D. Valdez-Balderas, M. A. Moore., P. Olsson, S. Teitel, Physical Review E, 83(3), 030303 (2011).
[23] When listing a function's arguments we place parameters that are held constant before the semicolon